Acriflavine Is More than It Seems: Resolving Optical Properties of Multiple Isomeric Constituents at 5 K

Alexander Schäfer,[§] Sreekanta Debnath,*[,§] Jana Tränkle, Theresa Mohr, and Manfred M. Kappes*

ABSTRACT: Ion mobility spectrometry at room temperature was combined with vibrationally resolved electronic spectroscopy of mass-selected ions at 5 K to study the well-known cationic fluorophore acriflavine. One- and two-color photodepletion action spectra recorded in gas-phase (by helium tagging) as well as dispersed fluorescence spectra obtained in neon matrix (after soft-landing deposition) indicate that the primary cation mass electrosprayed from solution comprises two isomers with different optical properties. Theory at the TD-DFT level allowed full spectral assignment. The results have implications for the preparation of novel thin film photonic materials by low-energy ion beam deposition.

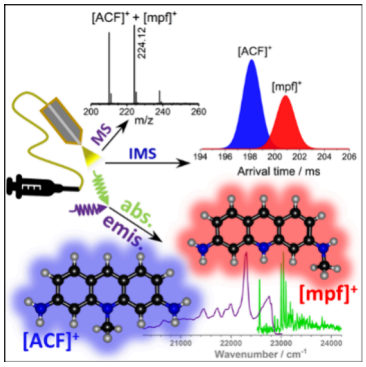

Molecular fluorophores whose optical properties are expected to change significantly with charge state are presently being explored for various applications ranging from photoredox catalysis,[1] chemical sensing, through LED devices to quantum optics.[2−4] A prerequisite for this is that the environmental interactions of the chromophore are well understood and can be controlled—ideally on molecular length scales. One promising recent approach toward this is light emission STM under cryogenic conditions to probe electroluminescence as a function of charge states down to the single molecule level.[5,6] For these and related charge state dependent studies, environmental control is realized by depositing the fluorophores from the gas phase onto clean (insulating) surfaces under ultrahigh vacuum conditions.[7] Many of the most interesting fluorophores are photochemically robust in the condensed phase but are too labile to be transferred to clean surfaces by sublimation. Electrospray ionization (ESI) followed by mass selective low energy ion beam deposition (soft-landing) offers an alternative approach, particularly for fluorophores which readily form ions in solution.[8−10]

We have recently used mass-selective ESI deposition to soft-land samples of both Rhodamine B[11] and Pyronin Y[12] dye cations into a (codeposited) neon cryomatrix. Laser-induced visible region dispersed photoluminescence (PL) spectra of these matrix isolated species were compared to the absorption spectra of the corresponding cations in gas-phase as measured via helium tagging photodepletion spectroscopy (He-TAG PD). This approach of recording vibronically resolved absorption and emission spectra at 5 K in combination with theoretical predictions allows to establish the exact nature and charge state of the emitting species as well as to assign the associated transitions to high spectroscopic accuracy.

Organic dyes obtained from commercial sources are oftentimes contaminated by side products that are generated during their multistep synthesis. While mass-selective deposition eliminates those side products having different mass, (equi m/z) isomers of the ions of interest can still present problems. On the other hand, strongly fluorescent but spectrally distinguishable isomers offer additional application perspectives if their on-surface ratios can be quantified and ultimately controlled. In this contribution, we present a study of such a case: acriflavine, an antibacterial chromophore well studied in condensed phase (see overview in next paragraph). Specifically, we use a combination of ESI mass spectrometry, ion mobility spectrometry (IMS), one- and two-color He-TAG PD (allowing for isomer hole burning), PL of mass-selected ions deposited into neon as well as TD-DFT calculations of the corresponding S_0-S_1 electronic transitions to deconvolute and definitively assign the vibrationally resolved electronic spectra to two coexisting isomers with distinctly different optical properties.

Acriflavinium chloride (3,6-diamino-10-methylacridin-10-ium chloride; see Scheme 1) also commonly known as acriflavine, was first introduced in 1912 as an antiseptic by the German scientist Paul Ehrlich.[13,14] Since then samples of acriflavine have been extensively used mainly in biological and

Scheme 1. Structures of the Fluorescent Isomeric Cations of Interest in This Study: 3,6-Diamino-10-methylacridin-10-ium ([ACF]$^+$; "Acriflavinium") and Its Isomer (protonated) 3-Amino-6-(methylamino) Acridin-10-ium ([mpf]$^+$, "Methylproflavinium")[a]

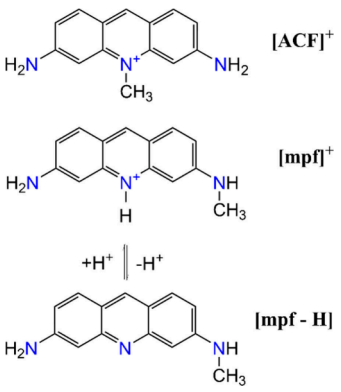

[a]In a protic solvent [**mpf**]$^+$ can be in equilibrium with its neutral deprotonated form: 3-amino-6-(methylamino)-acridine ([**mpf-H**]).

biomedical applications,[15−17] among others - typically in the form of aqueous solutions.[18−20] Acriflavine is in fact one of the most commonly studied cationic acridine dyes. Nevertheless, despite numerous applications related to its strong visible region absorption and fluorescence, the spectroscopic description of this dye in the condensed/solution phase is still surprisingly incomplete and even inconsistent among different studies. For example, the position and intensity of absorption and emission features, differ significantly in the published room temperature spectra of acriflavine recorded in aqueous solution.[21−23] Manivannan et al.[22] reported $^{abs}\lambda_{max}$ and $^{emis}\lambda_{max}$ at 449 and 510 nm, whereas, Sharma et al.[23] measured them to be at 416 and 514 nm, respectively. Part of the problem lies in the fact that the commercially available material has long been known to contain not only 3,6-diamino-10-methylacridin-10-ium chloride but also a spectroscopically distinct proflavine (acridine-3,6-diamine) impurity in varying amounts depending on supplier and batch. While exploring the use of acriflavine as a fluorescent dye for cell sorting (it is reported to intercalate into DNA), Tiffe et al.[24] used NMR and LC-MS to show that commercial samples typically also contain some unspecified bimethylated derivatives in addition to the proflavine impurity. Subsequently, while analyzing veterinary drug residues in fish aquacultures Turnipseed et al.[25] observed two chromatographically separable isomers detectable by mass spectrometry at the mass-to-charge ratio corresponding to the acriflavinium ion (m/z = 224.12). No further structural assignment of these isomers was however carried out. Very recently, Napolitano et al.[17] studied the potential of acriflavine (which is a clinically approved drug in some countries), as an effective inhibitor of SARS-CoV-2 papain-like protease (PLpro). As part of their study which used a commercial acriflavine sample, they performed HPLC-MS-based analytics (presumably with ESI), and inferred that their solutions comprised at least four different cationic molecular species, including two isomers at "m/z= 224.29". These were assigned as 3,6-diamino-10-methylacridin-10-ium and 3-amino-6-(methylamino)-acridin-10-ium based on ^{1}H NMR. These two isomeric structures are shown in Scheme 1. 3,6-diamino-10-methylacridin-10-ium, is the molecule commonly thought to be the cationic constituent of acriflavine. It is characterized by a methyl group attached to the central endocyclic 'N' of the acridine ring. In the following we will abbreviate it as [ACF]$^+$. By contrast, in 3-amino-6-(methylamino)-acridin-10-ium, the methyl group is substituted at the side amine moiety. Below we will call it [mpf]$^+$ to distinguish it from the main acriflavine isomer [ACF]$^+$. Scheme 1 additionally shows that in protic solution [mpf]$^+$ can also exist in equilibrium with its deprotonated and thereby neutralized form, 3-amino-6-(methylamino)-acridine, [mpf-H]. This will also become relevant in the following.

There are as of yet no in-depth gas-phase studies of the acriflavine cation family apart from a collision cross section (CCS) value determined for the m/z = 224.12 ion ($^{TW}CCS_{N2}$ = 146.3 Å^2) electrosprayed from polar solution using a traveling wave instrument with comparatively low ion mobility resolution.[26,27] Furthermore, Dobbie et al.[28] have shown that the cationic m/z = 224 component of ESI-sprayed commercial acriflavine is a strong fluorophore also in gas-phase and have reported its fluorescence excitation and emission spectrum upon electrodynamic trapping at room temperature in ~10^{-3} mbar of helium bath gas.

To explore this system, we first analyzed a commercial acriflavine sample (Sigma-Aldrich, see SI for details) by both

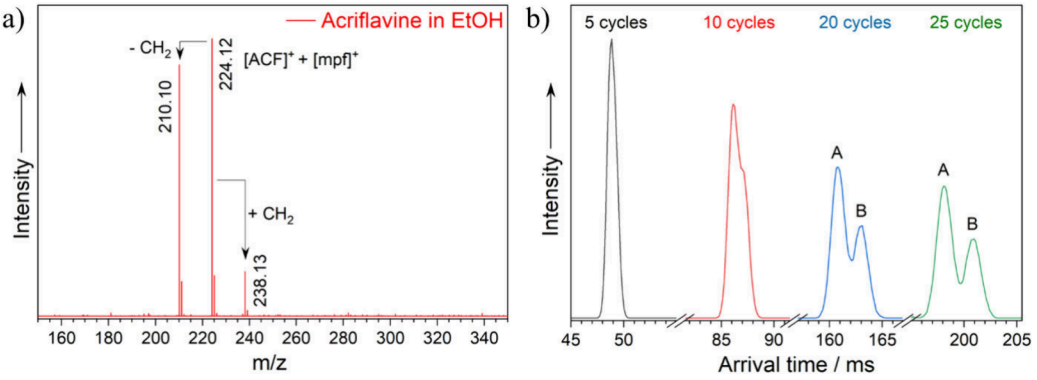

Figure 1. a) Mass spectrum of a commercial acriflavine sample (10^{-5} M) electrosprayed from ethanol solution. Note the presence of major signals at m/z = 210.10, 224.12, and 238.13 corresponding to distinct cationic chromophores present in solution (see text and SI). We focus on m/z = 224.12 species in this study. b) Arrival time distributions of m/z = 224.12 measured by cyclic ion mobility as a function of the number of separation cycles. Note the clear ion mobility separation of two isomers, labeled **A** and **B**. These correspond to 3,6-diamino-10-methylacridin-10-ium, [ACF]$^+$, and its isomer (protonated) 3-amino-6-(methylamino)-acridin-10-ium, [mpf]$^+$ (Scheme 1).

mass spectrometry and high-resolution cyclic ion mobility spectrometry - for details of this room temperature measurement see SI. In line with ref 17, the mass spectrum plotted in Figure 1a shows the presence of three major cationic constituents with mass-to-charge (m/z) ratios of 210.10, 224.12, and 238.13. We checked each of them for coexisting isomers and tautomers by recording m/z-resolved arrival time distributions following procedures described in detail elsewhere[29] (see also its SI). Figure 1b shows the results for the m/z = 224.12 ion packet corresponding to the mass of interest here. This contains two resolvable isomers with collision cross sections ($^{TW}CCS_{N2}$) of 147.7 Å^2 (peak **A**) and 148.4 Å^2 (peak **B**). Simulated collision cross sections ($^{theo}CCS_{N2}$) of 148.9 Å^2 for $[ACF]^+$ and 149.2 Å^2 for $[mpf]^+$ are in very good agreement (<1% difference) with the experimental values. This suggests, that the more abundant (and slightly more compact) isomer (peak **A**) has the "classical" acriflavine structure with a methylated endocyclic N atom (see Scheme 1; $[ACF]^+$). The slightly larger, lower intensity isomer (peak **B**), has a singly methylated amino group and is protonated on its central endocyclic N (see Scheme 1; $[mpf]^+$). (For completeness we note that the two impurity masses seen in Figure 1a correspond respectively to proflavine protonated at its endocyclic nitrogen (m/z 210.10) and bimethylated proflavine (m/z 238.13) − as also assigned in ref 17 by ^{1}H NMR. Corresponding arrival time distributions and experimental $^{TW}CCS_{N2}$ values as well as schematic molecular structures can be found in Figure S1).

It is important to note at this point, that the relative intensities of the peaks in the respective ion arrival time distributions shown in Figure 1b correspond to the gas phase isomer compositions−in this case, of $[ACF]^+$ versus $[mpf]^+$. These may differ considerably from the ratios in solution due for example to the availability of excess protons or hydroxyl groups in the respective solvents and/or due to electrochemical reactions associated with the ESI process.[30] Nevertheless, various studies have shown that ESI ionization efficiency by protonation correlates with basicity of the protonation site and solution pH, e.g. ref 31. To test this, arrival time distributions for the m/z 224.12 feature were measured by electrospraying acriflavine samples from different solvents. A notable increase in relative intensity of $[mpf]^+$:$[ACF]^+$ is observed upon using protic solvents (H_2O and EtOH) over an aprotic solvent (acetonitrile), see Table S1. Moreover, when excess NaOH was added to the solution in protic solvent, only one peak (isomer **A**) was observed in the mass resolved arrival time distribution, i.e. the protonated $[mpf]^+$ species effectively disappears (see Figure S4). This provides strong support for the assignment of peaks **A** and **B** in Figure 1b to $[ACF]^+$ and $[mpf]^+$ isomers, respectively.

Next, we will move on to the electronic spectroscopy of $[ACF]^+$ and $[mpf]^+$ which we typically studied using an isomer mixture (commercial acriflavine sample). First, we attempted to reproduce the solution phase spectra of acridinium hydrochloride by measuring UV−vis spectra of a 3 × 10^{-5} M aqueous solution at room temperature. This yielded an $^{abs}\lambda_{max}$ of 449 nm (see Figure S5) in agreement with Manivannan et al.[22] but in contradiction to Sharma et al.[23] - highlighting the compositional variability of the material as obtained from different commercial sources. To acquire better-defined insights into the vibronic features of the absorption spectra we then recorded vibrationally resolved PD spectra over the 410−465 nm spectral range at 5 K using the He-TAG PD method (see Figure S6). Specifically, we prepared and probed $[ACF•He]^+$ and $[mpf•He]^+$ each with a single helium atom tag as ascertained by mass spectrometry, i.e. m/z = 224 + 4 = 228. Strong depletions were observed in the 410−445 nm region as shown in the panel (a) of Figure 2 (in blue). SI

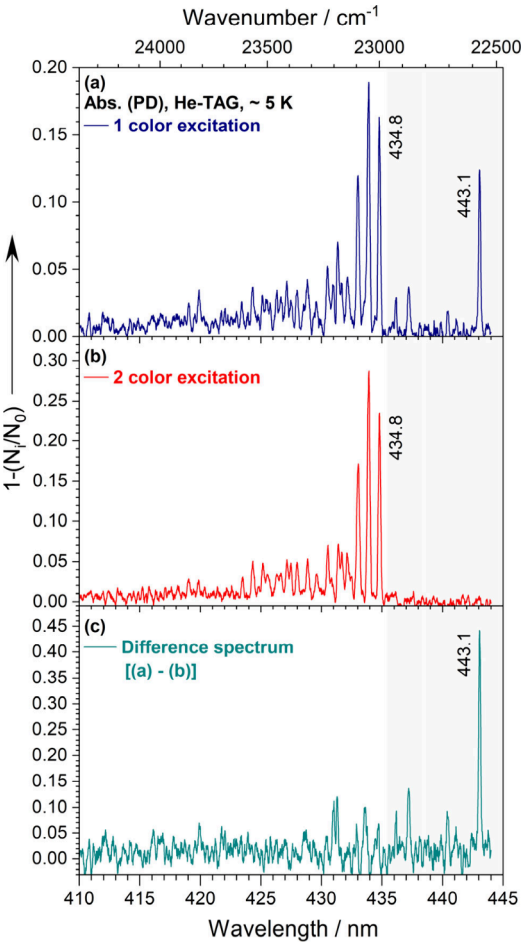

Figure 2. Vibrationally resolved gas-phase PD spectra of $[ACF•He]^+$ and $[mpf•He]^+$, i.e. each isomer tagged with a single He atom and probed at ca. 5 K. (a) 1-color PD spectrum showing a superposition of both isomers (blue); (b) 2-color PD spectrum (red) - acquired by setting one laser to 443.1 nm (and thus depleting $[mpf•He]^+$) while scanning the second laser to record the spectrum of $[ACF•He]^+$ selectively. (c) Difference spectrum (green), (b)-(a), showing the intrinsic PD spectrum of $[mpf•He]^+$, i.e. the isomer with $^{00}\nu$ at 443.1 nm (see SI for details).

provides further details (including a measurement extending to 465 nm showing no measurable depletion above the noise limit beyond 443.1 nm). Note that two distinct sets of spectral features can be seen in Figure 2 which we assign to a superposition of $[ACF]^+$ and $[mpf]^+$ absorptions−assuming to first order that (i) depletion cross sections correspond to absorption cross sections and (ii) He-atom induced spectral shifts are negligible.[11,12] Starting from the red, an intense and sharp absorption peak appears at 443.1 nm (22571 cm^{-1}), followed by multiple peaks with weaker depletions. Subsequently, three significantly more intense absorptions positioned at 434.8 nm (23000 cm^{-1}), 433.9 nm (23048 cm^{-1}), and 433.0 nm (23094 cm^{-1}) can be seen, followed by a weaker vibronic progression to shorter wavelength (Table S2 lists all the peak positions).

In Figure S8 our 5 K PD spectrum of $[ACF•He]^+$ and $[mpf•He]^+$ is compared with the previously determined room temperature fluorescence excitation spectrum of trapped "acriflavine m/z = 224" ions as measured by Dobbie et al.[28] Whereas the PD spectrum shows sharp intense absorptions (with fwhm's ranging 9.7 cm^{-1} to 12.8 cm^{-1} for the most intense peaks) associated with vibronic progression, the room temperature fluorescence excitation spectrum appears broad and unresolved. Furthermore, the highest intensity peak of the PD spectrum (λ_{max} = 433.9 nm) is ~11 nm blue-shifted w.r.t. the fluorescence excitation spectrum (λ_{max} = 445 nm). This is as expected owing to the lower thermal energy of the ions in the He-TAG experiment (and therefore reduced population of vibrationally excited electronic ground state species[12]). Interestingly though, while the two distinctive sets of absorption features in our PD spectrum are not resolved in their fluorescence excitation spectrum, Dobbie et al. recorded a DF spectrum showing two partially resolved emission bands (discussed later).[28]

To prove the attribution of the 5 K PD spectrum shown in panel (a) of Figure 2 to a superposition of $[ACF]^+$ and $[mpf]^+$ isomers and to distinguish between their spectroscopic signatures, the instrumental setup of the He-TAG experiment was next tailored to perform vis/vis-2-color excitation spectroscopy ("isomer hole burning"). A detailed description of this setup is given in the SI. In brief, the first laser was set to 443.1 nm, the longest wavelength feature in the PD spectrum, so as to untag the corresponding isomer. Under these conditions the other isomer which constituted roughly 62% of the total ion signal does not absorb and remains tagged with He. The second laser was then scanned to record the absorption spectrum of the remaining tagged isomer (via its depletion) while continuing to completely burn away the other isomer absorbing at 443.1 nm. Thereby, a pure PD spectrum of a second isomer with a band origin ($^{00}\nu$) at 434.8 nm is obtained without any contribution from the first isomer—as shown in the panel (b) of Figure 2 (in red). A clear background in the 445–435 nm range (missing absorption signatures) of Figure 2b confirms the complete dissociation of the first isomer by irradiation at 443.1 nm. The spectral signature of the isomer with $^{00}\nu$ at 443.1 nm can then be simply obtained by subtracting the panel (b) spectrum from that in panel (a) − to yield panel (c) of Figure 2. Note that the two isomers display different absorption profiles with stronger vibronic bands for ACF^+ than for mpf^+ which we attribute to the somewhat larger geometry change for excitation to S_1 in the case of ACF^+ (see also Figure S10). In summary, vis/vis-2-color excitation spectroscopy confirms the presence of two isomers at m/z = 224 and clearly identifies their associated vibronic transitions.

Vibronic information complementary to that shown in the PD spectrum was obtained by measuring DF spectra (using λ_{ex}: 405 nm) of electrosprayed and then mass-selected ($[ACF]^+$ + $[mpf]^+$) ions deposited onto a 5 K Ne matrix as shown in Figure 3 (in black; see Table S3 for peak positions). In line with the 5 K PD spectrum, two distinct sets of emission peaks separated by 9.7 nm (vs 8.3 nm in the PD spectrum) are obtained as plausible contributions from the two isomers. The Ne-matrix DF spectrum (λ_{ex}: 405 nm, in black) is compared with the He-tagged PD spectrum (in blue) in Figure S9. The PD spectrum shows significantly narrower peaks compared to the DF spectrum. This is due to the minimized environmental perturbation achieved under He-TAG experimental conditions.

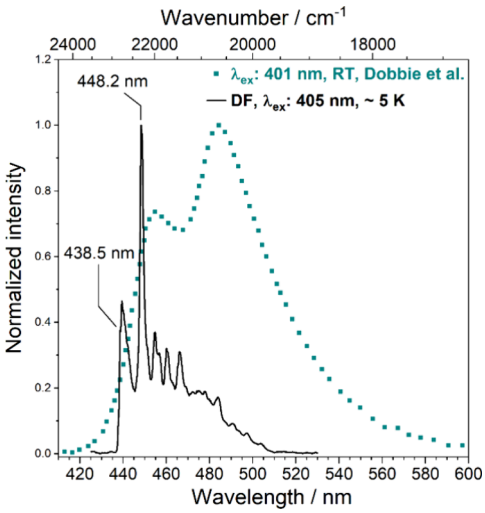

Figure 3. Vibrationally resolved DF spectrum of a mixture of $[ACF]^+$ and $[mpf]^+$ obtained upon depositing m/z = 224 ions onto/into a codeposited Ne matrix at ~5 K, using λ_{ex}: 405 nm (black). The spectrum is compared with the previously reported gas-phase DF spectrum of the same cationic species probed in a room temperature ion trap, using λ_{ex}: 401 nm (green), adapted from Dobbie et al.,[28] using parts of the data in Figure 2.3. Copyright [2023] [H. Dobbie].

Moreover, although the emission and absorption spectra do not form perfect mirror images, they show strong similarities. Considering the position and width of the peaks in the PD and DF spectrum, 22309 cm^{-1} (448.2 nm; DF) and 22571 cm^{-1} (443.1 nm; PD), and 22804 cm^{-1} (438.5 nm; DF) and 23000 cm^{-1} (434.8 nm; PD) transitions are likely to be arising from the same isomers. Therefore, the resulting blueshift of the PD spectrum w.r.t the DF spectrum, i.e. the combined effect of Stokes shifts and different experimental environments, is calculated to be 262 cm^{-1} (5.1 nm) and 196 cm^{-1} (3.7 nm), respectively. Comparing this blue shift with other matrix-isolated cationic dye systems reported by our group,[11,12] suggests that there is very little to almost no structural change upon excitation of each of the isomers to their respective higher electronic state (prior to fluorescence).

Figure 3 also compares our 5 K Ne matrix DF spectrum with the previously reported room temperature DF spectrum obtained for electrodynamically trapped gas-phase $[ACF]^+$ (+ $[mpf]^+$?) using λ_{ex}: 401 nm (in green) by Dobbie et al.[28] Compared to the gas-phase spectrum, the matrix spectrum shows sharper and vibrationally better-resolved emission peaks extending up to ~2000 cm^{-1} unveiling further vibrational information. Interestingly, both of the emission spectra (5 K and room temperature) show a dual emission feature with the peak in the red having higher intensity than the one in the blue (missing in the room temperature fluorescence excitation spectrum as already noted above (see blue curve in Figure S8)). The emission band maxima in the matrix spectrum appear at 448.2 nm (22309 cm^{-1}) and 438.5 nm (22804 cm^{-1}), ~ 37 nm and ~16 nm blue-shifted, respectively, compared to that of the gas-phase measurement. Note that the two emission bands of the room temperature DF spectrum had previously been tentatively assigned to arise from two close-lying electronic states (S_1 and S_2) of $[ACF]^+$.[28] By contrast, in our Ne-matrix spectrum we believe them to arise from the two different isomers $[ACF]^+$ and $[mpf]^+$ in correlation with our cyclic IMS and 2-color He-TAG PD experiments.

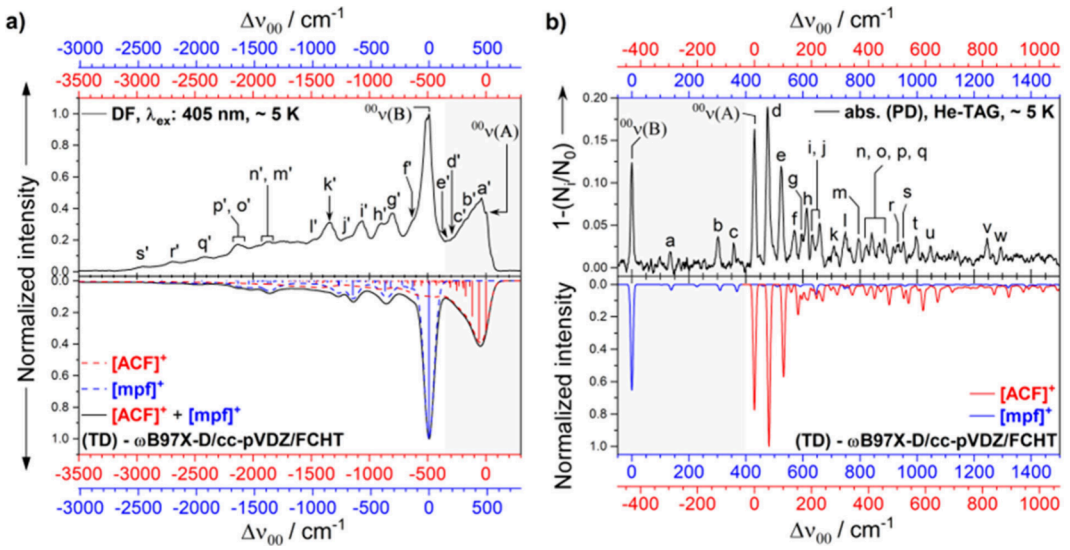

Figure 4. (a) Comparison of experimental 5 K neon matrix DF (top, in black) obtained with λ_{ex}: 405 nm and simulated emission spectrum of $[ACF]^+$ and $[mpf]^+$ broadened with a hwhm of 50 cm^{-1} (bottom). (b) Comparison of the experimental PD spectrum of $[ACF{\bullet}He]^+$ and $[mpf{\bullet}He]^+$ at ca. 5 K (top, in black) and simulated absorption spectrum broadened with a hwhm of 5 cm^{-1} (bottom). Simulated spectra are calculated at the (TD)-ωB97X-D/cc-pVDZ level of theory using the adiabatic Hessian AH-FCHT model. The relative intensities of the simulated spectra have been scaled to match the experimental findings due to different relative isomeric abundancies in the gas-phase and matrix samples. Different hwhm values chosen for the predicted DF and PD spectra are considered to match the corresponding broadening in the experimental spectra.

Optimized geometries (including bond lengths and angles) of both the $[ACF]^+$ and $[mpf]^+$ isomers in their ground (S_0) and first excited electronic state (S_1) are calculated at (TD)-ωB97X-D/cc-pVDZ level and presented in Figure S10a, b. Calculated vertical excitation energies at the same level of theory predicted the first excited singlet state (S_1) at 362.56 nm (f = 0.67) and 365.70 nm (f = 0.72) for $[ACF]^+$ and $[mpf]^+$, respectively (see Table S4 and S5). The dual absorption feature of the He-TAG PD spectrum with band origins ($^{00}\nu$) located at 434.8 and 443.1 nm satisfactorily agrees with this prediction (given the known error range of the computational method as applied to similar cationic chromophores), indicating both absorption features arise from the S_0-S_1 transition of the respective isomer. To further interpret the spectra and to facilitate the isomer-specific assignment of vibrational features, vibrationally resolved electronic absorption and emission spectra were calculated by applying the adiabatic Hessian (AH) model using the Franck–Condon-Herzberg–Teller (FCHT)[32] approximation. FCHT was chosen over FC as the former predicted slightly better agreement with our experimental spectra - in line with our previous studies of rigid cationic dyes.[11,12] The SI contains a detailed discussion of the theoretical approach. In brief, among the tested density functional and basis set combinations, only ωB97X-D/cc-pVDZ and CAM-B3LYP/cc-pVDZ yielded very good agreement with the experimental band origins ($^{00}\nu$) and vibronic progressions for both the isomers (see Figure S11–14). Figure 4a and b compares the isomer-specific experimental (top panels) and predicted (bottom panels) vibronic spectra (see Table S2 and S3 for band positions and assignments). The 0–0 band origin ($^{00}\nu$) is predicted at 26180 cm^{-1} (382 nm) and 25977 cm^{-1} (385 nm) for $[ACF]^+$ and $[mpf]^+$, respectively, ~ 15% blue-shifted from the Ne matrix DF and He-tagged PD spectra. Despite the shifted band origin, the vibrational progressions of the predicted spectra are, in very good agreement with the DF and PD spectra. Note that the predicted spectra plotted in Figure 4 are unscaled regarding the wavenumber and only (uniformly) shifted w.r.t. their band origins. Looking at the comparison in Figure 4, the set of absorption (PD) peaks with $^{00}\nu$ at 434.8 nm (438.5 nm in matrix DF) followed by a progression of two sharp intense and several less-intense vibrational features can unambiguously be assigned to arise from $[ACF]^+$. These intense peaks in the PD spectrum involve a symmetric out-of-plane vibrational mode at +47 cm^{-1} (peak 'd') and its first overtone peak 'e' at +94 cm^{-1} (see Figure S15). The other set of absorption peaks with $^{00}\nu$ at 443.1 nm in the PD spectrum (448.2 nm in matrix DF) can be assigned to $[mpf]^+$.

Note that in addition to the cis conformational isomer of $[mpf]^+$ discussed so far there is a less stable trans rotamer having the same bond connectivity but with its in-plane N–CH_3 bond rotated by 180 deg (see Scheme 1 and Figure S16). The calculated barrier for cis–trans interconversion is on the order of 0.7 eV so that both forms might be present in equilibrium in room temperature solution. However, the vibronic structure predicted for the trans rotamer is in much poorer agreement with the He-TAG spectrum and it therefore does not significantly contribute to the gas-phase measurement (at 5 K).

To date, the broad room temperature optical absorption/emission features of acriflavine (as studied in solution and more recently also in gas-phase) have generally been assigned only to 3,6-diamino-10-methylacridin-10-ium $[ACF]^+$.[22,23,28] In line with the recent (HP)LC-MS studies of Turnipseed et al.[25] and Napolitano et al.[17] we demonstrate that ESI of solvated acriflavine (from a commercial supplier) yields two spectroscopically distinct structural isomers at the primary cation mass m/z = 224.12. Upon isolation (for PD in gas-phase, for DF in neon) and cooling to 5 K, both isomers show vibrationally well-resolved PD and DF spectra which allow us to clearly assign their 0–0 band origins ($^{00}\nu$). While easily

distinguishable in our experiments they are close enough spectrally ($\Delta^{00}\nu$ = 429 and 495 cm^{-1} for PD and DF, respectively) such that their associated upper state vibrational progressions are partially interleaved/overlapped. In a modified He-TAG experiment involving vis-vis 2-color irradiation of the $[ACF{\bullet}He]^+$ and $[mpf{\bullet}He]^+$ mixture with separately tunable pulsed lasers we therefore selectively depleted one of the two isomers which allowed us to explicitly determine the full PD spectrum of the other isomer. Comparison with TD-DFT predictions of S_0-S_1 respectively S_1-S_0 transitions using the FCHT method yields satisfactory agreement, allowing the assignment of all experimentally distinguishable vibronic transitions (S/N ratios >2) to a specific isomer.

As reported by us for other fluorophores,[11,12,33,34] we have observed that both $[ACF]^+$ and $[mpf]^+$ can also undergo some charge changing during soft-landing deposition into neon, resulting in strongly fluorescent *neutrals* which emit significantly to the red of their charged precursors when excited in the UV. We will report details in a future study.[35] Consequently, ESI soft-landing of "acriflavinium ion m/z= 224" can generate at least four distinct fluorophores (two charged and two neutral isomers—possibly also with contributions from both $[mpf]^+$ rotamers). Furthermore, their relative amounts can be varied by adjusting neutralization efficiencies (via codoping of the matrix with electron getters to enhance cations) as well the cationic isomer ratios incident from the gas phase. Above we have shown that $[mpf]^+$ can be removed from the incident ion beam (and therefore selectively blocked from depositing onto the surface) by spraying from basic solution. By contrast pure beams of $[ACF]^+$ could be generated by bulk scale chromatographic separation along the lines of ref 17 - prior to ESI. In combination with a dual needle ESI-MS deposition setup,[36] it should therefore be possible, e.g., to structure adjacent stripes of the two charged isomers on a surface (via ion beam focusing and masking) or to generate vertically alternating layers of them in codeposited neon. This would allow to probe photophysical interactions between at least four well-defined fluorophores on length scales of less than 100 nm. Interestingly, the proton attached to the endocyclic nitrogen of $[mpf]^+$ is retained upon soft-landing. Thus, photoinduced proton transfer processes could also be studied.

An alternative approach to sequentially depositing prepurified isomers by dual needle ESI-MS would be to mobility select them after ESI-MS but prior to deposition. While ESI-MS-IMS is well established for isomer-selective electronic or vibrational spectroscopy,[37−40] mass *and* isomer-selective soft-landing remains to be demonstrated. In the present case of acriflavine ($[ACF]^+$ + $[mpf]^+$), a CCS resolution (CCS/ΔCCS) of significantly greater than 200 would be required to baseline separate isomers by ion mobility filtering. This is doable with present technology but requires optimization to ensure sufficient ion dose. Finally, the approach outlined here is also applicable to fragment ions. For example, the primary CID fragmentation channel of $[ACF]^+$ is CH_3 loss—presumably from the endocyclic N to form the proflavine radical cation. It would be interesting to probe the structure and electronic spectroscopy of this and related species both in the gas phase and in the cryomatrix.

In conclusion, we have probed the electronic spectroscopy of the cationic fluorophore acriflavine at 5K in isolation. One- and two-color photodepletion action spectra as well as dispersed fluorescence spectra indicate that the primary cation mass comprises two isomers with different optical properties. Theory at the TD-DFT level allows full spectral assignment.

AUTHOR INFORMATION

Corresponding Authors

Sreekanta Debnath − *Institute of Physical Chemistry II, Karlsruhe Institute of Technology, 76131 Karlsruhe, Germany;* orcid.org/0000-0001-9585-1876; Email: debnathsreekanta50@gmail.com

Manfred M. Kappes − *Institute of Physical Chemistry II, Karlsruhe Institute of Technology, 76131 Karlsruhe, Germany; Institute of Nanotechnology, Karlsruhe Institute of Technology, 76344 Eggenstein-Leopoldshafen, Germany;* orcid.org/0000-0002-1199-1730; Email: manfred.kappes@kit.edu

Authors

Alexander Schäfer − *Institute of Physical Chemistry II, Karlsruhe Institute of Technology, 76131 Karlsruhe, Germany;* orcid.org/0000-0002-2392-3217

Jana Tränkle − *Institute of Physical Chemistry II, Karlsruhe Institute of Technology, 76131 Karlsruhe, Germany*

Theresa Mohr − *Institute of Physical Chemistry II, Karlsruhe Institute of Technology, 76131 Karlsruhe, Germany*

Author Contributions

§ A.S. and S.D. contributed equally to this work.

Notes

The authors declare no competing financial interest.

ACKNOWLEDGMENTS

This research was supported by DFG under projects C1 and C3 of the CRC 1573 "4f-for-future". We also thank DFG and KIT for funding of a Cyclic IMS (Art. 91b GG). S.D. and A.S. acknowledge support by the state of Baden-Württemberg through bwHPC and the German Research Foundation (DFG) through Grant No. INST 40/575-1 FUGG (JUSTUS 2 cluster). We thank Patrick Weis for his help with the Cyclic IMS.

REFERENCES

(1) Tlili, A.; Lakhdar, S. Acridinium Salts and Cyanoarenes as Powerful Photocatalysts: Opportunities in Organic Synthesis. *Angew. Chem., Int. Ed.* **2021**, *60* (36), 19526−19549.

(2) Musavinezhad, M.; Shkarin, A.; Rattenbacher, D.; Renger, J.; Utikal, T.; Götzinger, S.; Sandoghdar, V. Quantum Efficiency of Single Dibenzoterrylene Molecules in P-Dichlorobenzene at Cryogenic Temperatures. *J. Phys. Chem. B* **2023**, *127* (23), 5353−5359.

(3) Neumann, M.; Wei, X.; Morales-Inostroza, L.; Song, S.; Lee, S.-G.; Watanabe, K.; Taniguchi, T.; Götzinger, S.; Lee, Y. H. Organic Molecules as Origin of Visible-Range Single Photon Emission from Hexagonal Boron Nitride and Mica. *ACS Nano* **2023**, *17* (12), 11679−11691.

(4) Zirkelbach, J.; Mirzaei, M.; Deperasińska, I.; Kozankiewicz, B.; Gurlek, B.; Shkarin, A.; Utikal, T.; Götzinger, S.; Sandoghdar, V. High-Resolution Vibronic Spectroscopy of a Single Molecule Embedded in a Crystal. *J. Chem. Phys.* **2022**, *156* (10), 104301.
(5) Jiang, S.; Neuman, T.; Bretel, R.; Boeglin, A.; Scheurer, F.; Le Moal, E.; Schull, G. Many-Body Description of Stm-Induced Fluorescence of Charged Molecules. *Phys. Rev. Lett.* **2023**, *130* (12), No. 126202.
(6) Rai, V.; Gerhard, L.; Sun, Q.; Holzer, C.; Repän, T.; Krstić, M.; Yang, L.; Wegener, M.; Rockstuhl, C.; Wulfhekel, W. Boosting Light Emission from Single Hydrogen Phthalocyanine Molecules by Charging. *Nano Lett.* **2020**, *20* (10), 7600−7605.
(7) Rai, V.; Gerhard, L.; Balzer, N.; Valášek, M.; Holzer, C.; Yang, L.; Wegener, M.; Rockstuhl, C.; Mayor, M.; Wulfhekel, W. Activating Electroluminescence of Charged Naphthalene Diimide Complexes Directly Adsorbed on a Metal Substrate. *Phys. Rev. Lett.* **2023**, *130* (3), No. 036201.
(8) Kern, B.; Greisch, J.-F. o.; Strelnikov, D.; Weis, P.; Böttcher, A.; Ruben, M.; Schäfer, B.; Schooss, D.; Kappes, M. M. Photoluminescence Spectroscopy of Mass-Selected Electrosprayed Ions Embedded in Cryogenic Rare-Gas Matrixes. *Anal. Chem.* **2015**, *87* (23), 11901−11906.
(9) Hauptmann, N.; Hamann, C.; Tang, H.; Berndt, R. Soft-Landing Electrospray Deposition of the Ruthenium Dye N3 on Au (111). *J. Phys. Chem. C* **2013**, *117* (19), 9734−9738.
(10) Rauschenbach, S.; Stadler, F. L.; Lunedei, E.; Malinowski, N.; Koltsov, S.; Costantini, G.; Kern, K. Electrospray Ion Beam Deposition of Clusters and Biomolecules. *Small* **2006**, *2* (4), 540−547.
(11) Debnath, S.; Schäfer, A.; Haupa, K. A.; Strelnikov, D.; Roithová, J.; Jašík, J.; Lebedkin, S.; Kappes, M. M. Vibrationally Resolved Electronic Spectroscopy of Rhodamine B Cation at Less Than 5 K: Combining Gas Phase Absorption and Matrix Isolation Fluorescence Spectroscopy. *Mol. Phys.* **2023**, *122* (1−2), No. e2223072.
(12) Debnath, S.; Schäfer, A.; Ito, S.; Strelnikov, D.; Schneider, R.; Haupa, K. A.; Kappes, M. M. Vibrationally Resolved Absorption, Fluorescence, and Preresonance Raman Spectroscopy of Isolated Pyronin Y Cation at 5 K. *J. Phys. Chem. Lett.* **2023**, *14* (47), 10553−10560.
(13) Browning, C. The Treatment of Wounds by Flavine. *BMJ.* **1918**, *1* (2984), 301.
(14) Benda, L. Über Das 3.6-Diamino-Acridin. *Dtsch. Chem. Ges.* **1912**, *45* (2), 1787−1799.
(15) Nehme, R.; Hallal, R.; El Dor, M.; Kobeissy, F.; Gouilleux, F.; Mazurier, F.; Zibara, K. Repurposing of Acriflavine to Target Chronic Myeloid Leukemia Treatment. *Curr. Med. Chem.* **2021**, *28* (11), 2218−2233.
(16) Wainwright, M. Acridine - a Neglected Antibacterial Chromophore. *J. Antimicrob. Chemother.* **2001**, *47* (1), 1−13.
(17) Napolitano, V.; Dabrowska, A.; Schorpp, K.; Mourão, A.; Barreto-Duran, E.; Benedyk, M.; Botwina, P.; Brandner, S.; Bostock, M.; Chykunova, Y. Acriflavine, a Clinically Approved Drug, Inhibits Sars-Cov-2 and Other Betacoronaviruses. *Cell Chem. Biol.* **2022**, *29* (5), 774−784.e778.
(18) Li, Y.; Wang, A.; Bai, Y.; Wang, S. Acriflavine-Immobilized Eggshell Membrane as a New Solid-State Biosensor for Sudan I−Iv Detection Based on Fluorescence Resonance Energy Transfer. *Food Chem.* **2017**, *237*, 966−973.
(19) Misra, V.; Mishra, H.; Joshi, H.; Pant, T. Excitation Energy Transfer between Acriflavine and Rhodamine 6g as a Ph Sensor. *Sens. Actuators B Chem.* **2000**, *63* (1−2), 18−23.
(20) Wang, X.-d.; Wolfbeis, O. S. Optical Methods for Sensing and Imaging Oxygen: Materials, Spectroscopies and Applications. *Chem. Soc. Rev.* **2014**, *43* (10), 3666−3761.
(21) Ladoulis, C. T.; Gill, T. J., III Physcial Chemical Studies on the Specific Interaction of an Acriflavine-Phosphotungstic Acid Complex with Double-Stranded Nucleic Acids. *J. Cell Biol.* **1970**, *47* (2), 500−511.
(22) Manivannan, C.; Meenakshi Sundaram, K.; Sundararaman, M.; Renganathan, R. Investigation on the Inclusion and Toxicity of Acriflavine with Cyclodextrins: A Spectroscopic Approach. *Spectrochim. Acta - A: Mol. Biomol. Spectrosc.* **2014**, *122*, 164−170.
(23) Sharma, V. K.; Sahare, P. D.; Rastogi, R. C.; Ghoshal, S. K.; Mohan, D. Excited State Characteristics of Acridine Dyes: Acriflavine and Acridine Orange. *Spectrochim. Acta - A: Mol. Biomol. Spectrosc.* **2003**, *59* (8), 1799−1804.
(24) Tiffe, H.; Matzke, K.; Thiessen, G. The Acridine Dyes: Their Purification, Physicochemical, and Cytochemical Properties: Ii. Purification of Acriflavine and Proflavine and Their Cytochemical Behaviour Regarding Machine-Oriented Evaluation. *Histochemistry* **1977**, *53* (1), 63−77.
(25) Turnipseed, S. B.; Storey, J. M.; Wu, I.-L.; Andersen, W. C.; Madson, M. R. Extended Liquid Chromatography High Resolution Mass Spectrometry Screening Method for Veterinary Drug, Pesticide and Human Pharmaceutical Residues in Aquaculture Fish. *Food Addit. Contam. A* **2019**, *36* (10), 1501−1514.
(26) *CCSBase*. https://ccsbase.net/results (accessed 26.06.2024).
(27) Hines, K. M.; Ross, D. H.; Davidson, K. L.; Bush, M. F.; Xu, L. Large-Scale Structural Characterization of Drug and Drug-Like Compounds by High-Throughput Ion Mobility-Mass Spectrometry. *Anal. Chem.* **2017**, *89* (17), 9023−9030.
(28) Dobbie, H. H. Intrinsic Photophysical Properties of Gaseous Acriflavine Ions. Master's Thesis, University of Toronto, 2023. https://hdl.handle.net/1807/128044.
(29) Hennrich, F.; Ito, S.; Weis, P.; Neumaier, M.; Takano, S.; Tsukuda, T.; Kappes, M. M. Cyclic Ion Mobility of Doped $[MAu_{24}L_{18}]^{2-}$ Superatoms and Their Fragments (M= Ni, Pd and Pt; L= Alkynyl). *Phys. Chem. Chem. Phys.* **2024**, *26* (10), 8408−8418.
(30) Ehrmann, B. M.; Henriksen, T.; Cech, N. B. Relative Importance of Basicity in the Gas Phase and in Solution for Determining Selectivity in Electrospray Ionization Mass Spectrometry. *J. Am. Soc. Mass Spectrom.* **2008**, *19* (5), 719−728.
(31) Oss, M.; Tshepelevitsh, S.; Kruve, A.; Liigand, P.; Liigand, J.; Rebane, R.; Selberg, S.; Ets, K.; Herodes, K.; Leito, I. Quantitative Electrospray Ionization Efficiency Scale: 10 Years After. *Rapid Commun. Mass Spectrom.* **2021**, *35* (21), No. e9178.
(32) Improta, R.; Barone, V.; Santoro, F. Accurate Steady-State and Zero-Time Fluorescence Spectra of Large Molecules in Solution by a First-Principle Computational Method. *J. Phys. Chem. B* **2007**, *111* (51), 14080−14082.
(33) Debnath, S.; Haupa, K. A.; Lebedkin, S.; Strelnikov, D.; Kappes, M. M. Triggering near-Infrared Luminescence of Vanadyl Phthalocyanine by Charging. *Angew. Chem.* **2022**, *134* (25), No. e202201577.
(34) Haupa, K. A.; Krappel, N. P.; Strelnikov, D.; Kappes, M. M. Vibrationally Resolved Absorption and Luminescence Spectra of Mass-Selected Free-Base and Zinc Phthalocyanine Radical Cations Isolated in Solid Ne. *J. Phys. Chem. A* **2022**, *126* (4), 593−599.
(35) Debnath, S.; Schäfer, A.; Kappes, M. M. Real Time Trapping of Reactive Radical Neutrals. *To be published*.
(36) Su, P.; Hu, H.; Warneke, J.; Belov, M. E.; Anderson, G. A.; Laskin, J. Design and Performance of a Dual-Polarity Instrument for Ion Soft Landing. *Anal. Chem.* **2019**, *91* (9), 5904−5912.
(37) Fromherz, R.; Ganteför, G.; Shvartsburg, A. A. Isomer-Resolved Ion Spectroscopy. *Phys. Rev. Lett.* **2002**, *89* (8), No. 083001.
(38) Vonderach, M.; Ehrler, O. T.; Weis, P.; Kappes, M. M. Combining Ion Mobility Spectrometry, Mass Spectrometry, and Photoelectron Spectroscopy in a High-Transmission Instrument. *Anal. Chem.* **2011**, *83* (3), 1108−1115.
(39) Masson, A.; Kamrath, M. Z.; Perez, M. A.; Glover, M. S.; Rothlisberger, U.; Clemmer, D. E.; Rizzo, T. R. Infrared Spectroscopy of Mobility-Selected H^+-Gly-Pro-Gly-Gly (Gpgg). *J. Am. Soc. Mass Spectrom.* **2015**, *26* (9), 1444−1454.
(40) Warnke, S.; Seo, J.; Boschmans, J.; Sobott, F.; Scrivens, J. H.; Bleiholder, C.; Bowers, M. T.; Gewinner, S.; Schollkopf, W.; Pagel, K.; von Helden, G. Protomers of Benzocaine: Solvent and Permittivity Dependence. *J. Am. Chem. Soc.* **2015**, *137* (12), 4236−4242.